

Soliton excitations as emitted clusters on nuclear surfaces

R. A. Gherghescu ^{1,2}, A. Ludu ¹, and J. P. Draayer ¹

¹ *Department of Physics and Astronomy, Louisiana State University, Baton Rouge LA 70803*

USA

² *National Institute of Physics and Nuclear Engineering, P.O. Box MG-6, RO-76900*

Bucharest-Magurele, Romania

Abstract

This work reports on calculations of the deformation energy of a nucleus plus an emitted cluster as a soliton moving on its surface. The potential barrier against the emission of a soliton is calculated within the macroscopic-microscopic method. The outer turning point of the barrier determines limitations on the geometrical and kinematical parameters for the formation of a surface soliton. For large asymmetry, the two-center shell model is used to assign a structure to the soliton. Calculations for ^{248}No with the emission of a ^{40}Ca soliton are reported; likewise for ^{224}Th with the emission of ^{16}O . Except for necked shapes at the very first stages of soliton formation, the greatest portion of the deformation path displays rather compact configurations with large neck radii. These shape sequences correspond to allowable soliton velocities. Close to and just beyond the touching point configuration, where the shape becomes concave, the width and the velocity of the soliton approach zero. The calculations suggest that the emission of a ^{40}Ca structure is quite probable due to a low potential barrier, whereas the emission of an ^{16}O type soliton is rather unlikely due to the higher penetration barrier.

I. INTRODUCTION

There are different theoretical models which describe cluster formation and emission from nuclei, and most of them use nonlinear partial differential equations. A fundamental understanding of nonlinear terms in a nuclear model reveals new phenomena and shapes more complicated than linear theory suggests. In this paper we introduce a model for the cluster emission, based on soliton solutions of nonlinear equation.

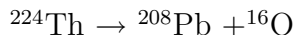
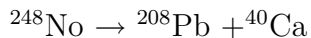
Soliton structures have been analyzed within the frameworks of hydrodynamics, nonlinear optics, solid state and plasma physics. Experimental and theoretical results [1] suggest that solitons are non-dispersive, localized waves executing uniform motion that can be described by three interrelated parameters: amplitude A , half-width L , and velocity V . Furthermore, these structures arise as analytical solutions of non-linear dynamical systems, like the Korteweg de Vries (KdV) or Nonlinear Schrödinger (NLS) equations. Soliton theory has been applied many times in nuclear physics, so far. For example, it provided very good descriptions of some localized stable surface excitations [2], of spectroscopic factors in cluster and α emission [3], and of quasimolecular spectra for α plus heavy nuclei collisions, [4]. Also, the cubic and quintic NLS equations were used in three-dimensional models for cluster emission [5], providing results in very good agreement with TDHF simulations.

In order to look for the possibility of describing nuclear phenomena such as cluster emission [6] by soliton formation on the nuclear surface, it is necessary to assign a microscopic structure to the parent heavy nucleus and the emitted soliton cluster. The microscopic substructure further allows one to add shell corrections to the usual macroscopic liquid drop energy and thus give a complete description of the system, from the initial nucleus with no soliton substructure to one with a soliton-like structure on its surface and on out to possible cluster emission.

A straightforward way to accomplish this is to calculate shell effects obtained from the

single-particle levels of an asymmetric two-center shell model. One of the centers is placed in the middle of a small emitted sphere and the other is the center of the heavy fragment. This approach allows a microscopic description of the nuclear evolution from one to two independent quantum systems.

The procedure involves calculating the total potential energy as the sum of the macroscopic energy and shell corrections which is then minimized, which yields a barrier that increases as a function of the amplitude of the soliton. Calculations have been performed for two possible reactions:



We select spherical daughters and emitted clusters, in order to fit the asymmetric two-center shell model we have constructed, which goes from one sphere (parent) to two necked spheres and then to separation.

In the present model, we describe cluster emission processes by using such soliton-like shapes on the nuclear surface of the heavy fragment. For a given cluster geometry, we calculate the corresponding soliton parameters (A , L , V) as functions of the separation parameter, that is along the static path of the cluster emission process.

Solitary waves have been shown recently to exist on liquid drops, bubbles, and shells [3]. The non-linear hydrodynamic equations are related with the KdV and mKdV equation generating localized patterns ranging from small oscillations to nonlinear ones, including solitons. This model has a Hamiltonian structure, and such soliton-like excitations were observed experimentally when the shape oscillations of a droplet became nonlinear. It is therefore natural to extend that this model to other drop-like systems, from neutron stars to hyperdeformed nuclei and fission.

In the first section we define the deformation space we that we work with and the shapes that can be obtained therein. In the second section we give a short description of the macroscopic-microscopic model we used in the calculations. Emphasis has been given on the asymmetric two-center shell model we constructed in order to approach solitonic shapes.

Results for the two reactions given above are presented in the third section.

II. SPACE OF DEFORMATION

The problem of describing cluster emission (or nuclear fission) by a convenient parametrization of the shape is not new, and it is a decisive factor determining the amount of calculations. In the present model we use a new type of parametrization, described by soliton shapes. As well as the other parametrizations are in relation with the nuclear system and its quantization, the soliton parametrization is related to the KdV and mKdV dynamics of the soliton. Moreover, the soliton model takes profit from the high stability in time of such shapes. While in general one associates solitons with macroscopic pictures, it is nevertheless true that the soliton dynamics can be quantized [1,2,4,7] and the KdV (or mKdV) equations can be related to quantum systems like those described by Schrödinger equations, [5,8], as we noted above.

Solitons on the surface are described by two asymmetrical spheres smoothly joined one to another through a neck region (Fig. 1). There are three independent geometrical parameters which form the space of deformation: the distance R between the centers of the two fragments, the emitted small sphere radius R_2 and the neck sphere radius R_3 . The neck region is obtained by rolling a sphere of radius R_3 around the symmetry axis. Such shapes are generated by the following equation written in cylindrical coordinates:

$$\rho(z) = \begin{cases} \sqrt{R_1^2 - (z - z_1)^2}, & z_1 - R_1 \leq z \leq z_{c1} \\ \rho_3 - \sqrt{R_3^2 - (z - z_3)^2}, & z_{c1} \leq z \leq z_{c2} \\ \sqrt{R_2^2 - (z - z_2)^2}, & z_{c2} \leq z \leq z_2 + R_2 \end{cases} \quad (1)$$

where the quantities not shown in Fig. 1 are: z_3 —the position of the center of the neck sphere on the symmetry axis, z_{c1} and z_{c2} —the positions of the intersection planes of the two fragments spheres with the neck sphere, and z_1 and z_2 —the positions of the two spherical fragment centers. The heavy fragment radius R_1 is obtained from total nuclear volume conservation. The soliton solution along the θ direction

$$r_{surface}(\phi, \theta, t) = A(\phi, t) \left[\operatorname{sech} \frac{\theta - Vt}{L} \right]^2 \quad (2)$$

is characterized by the amplitude A , or the relative amplitude $a = A/R_1$, the half-width L , and the angular velocity V . The soliton solutions have a special shape–kinematic dependence, $V \simeq A$ and $L \simeq 1/\sqrt{A}$, that is, a higher soliton is narrower and travels faster [1]. This relation can be used to experimentally distinguish solitons from other normal modes of excitations (for example by calculating the reciprocal moment of inertia) [3]. The amplitude of the soliton is related to the two-center shell model by the relation with $A = R - R_1 + R_2$. The halfwidth of the soliton is approximated with $2\rho(z_{c2})$, or with the diameter of the circular surface within the separation plane between the emitted sphere and the rest of the shape

$$L = \frac{2R_2A}{(1+a)(R_1 - R_2)}. \quad (3)$$

We mention that the cubic and quartic NLS equations are related to the mKdV equation by a very simple exponential transform, and actually there is no essential difference between the NLS and the mKdV solitons [1,8]. As an example, we notice the connection between the KdV equation and the nuclear potential in the Schrödinger equation [8], or the relation between NLS solitons and coherent states [7]. Some applications of the KdV or mKdV-solitons are macroscopic, but the soliton solutions can be quantified by standard procedures [1,4,9].

III. MACROSCOPIC ENERGY

The deformation energy E_{def} is calculated in a macroscopic-microscopic approach:

$$E_{def} = E_{macro} + \delta E_{shell} + \delta P. \quad (4)$$

The macroscopic part E_{macro} includes the shape-dependent components of the charged liquid drop:

$$E_{macro} = E_C + E_{Y+E}, \quad (5)$$

where E_C is the Coulomb energy and E_{Y+E} is the surface or nuclear energy calculated within the Yukawa-plus-exponential model [10,11].

The Coulomb energy general form is the double-volume integral:

$$E_C = \frac{1}{2} \int_V \int_V \frac{\rho_e(r_1)\rho_e(r_2)d^3r_1d^3r_2}{r_{12}}, \quad (6)$$

which is split into four parts, two of them being equal to one another [6]:

$$E_C = \frac{\rho_{1e}^2}{2} \int_{V_1} d^3r_1 \int_{V_1} \frac{d^3r_2}{r_{12}} + \rho_{1e}\rho_{2e} \int_{V_1} d^3r_1 \int_{V_2} \frac{d^3r_2}{r_{12}} + \frac{\rho_{2e}^2}{2} \int_{V_2} d^3r_1 \int_{V_2} \frac{d^3r_2}{r_{12}} \quad (7)$$

where $r_{12} = |r_1 - r_2|$. The first and the last terms represent the self-energies of the two fragments, and the middle term is the Coulomb interaction between the two fragments.

In cylindrical coordinates the three terms are given by:

$$\begin{aligned} E_c = & \frac{\rho_e^2}{10} \int_{z'}^{z''} dz \int_{z'}^{z''} dz_1 \int_0^{2\pi} d\varphi \int_0^{2\pi} d\varphi_1 \left(\rho^2 - \frac{z}{2} \frac{\partial \rho^2}{\partial z} \right) \left[\rho_1^2 - \right. \\ & \left. \rho \rho_1 \cos(\varphi - \varphi_1) + \rho \frac{\partial \rho_1}{\partial \varphi_1} \sin(\varphi - \varphi_1) + \frac{(z - z_1)}{2} \frac{\partial \rho_1^2}{\partial z_1} \right] \left[\rho^2 + \right. \\ & \left. \rho_1^2 - 2\rho \rho_1 \cos(\varphi - \varphi_1) + (z - z_1)^2 \right]^{-1/2}, \end{aligned} \quad (8)$$

where $\rho = \rho(z, \varphi)$ is the nuclear surface equation, and z' and z'' are the intersections of the surface with Oz axis.

The general form of the Yukawa-plus-exponential energy is:

$$E_{Y+E} = -\frac{a_2}{8\pi^2 r_0^2 a^4} \int_V \int_V \left(\frac{r_{12}}{a} - 2 \right) \frac{\exp(-r_{12}/a)}{r_{12}/a} d^3r_1 d^3r_2, \quad (9)$$

where $r_{12} = |\mathbf{r}_1 - \mathbf{r}_2|$, $a=0.68$ fm accounts for the finite range of nuclear forces, and $a_2 = a_s(1 - \kappa I^2)$. κ is the asymmetry energy constant, and the surface energy constant is $a_s=21.13$ MeV. In a similar way to the Coulomb part, one obtains three terms:

$$\begin{aligned} E_{Y+E} = & -\sum_{i=1}^2 \frac{a_{2i}}{8\pi^2 r_0^2 a^4} \int_{V_1} d^3r_1 \int_{V_1} \left(\frac{r_{12}}{a} - 2 \right) \frac{\exp(-r_{12}/a)}{r_{12}/a} d^3r_2 \\ & - \frac{2\sqrt{a_{21}a_{22}}}{8\pi^2 r_0^2 a^4} \int_{V_1} d^3r_1 \int_{V_2} \left(\frac{r_{12}}{a} - 2 \right) \frac{\exp -r_{12}/a}{r_{12}/a} d^3r_2 \end{aligned} \quad (10)$$

where $a_{2i} = a_s(1 - KI_i^2)$, $I_i = (N_i - Z_i)/A_i$. For shapes with axial symmetry, each of these terms involving a double-folded integration over the nuclear volume can be reduced to a three-dimensional integral.

IV. THE ASYMMETRIC TWO-CENTER SHELL MODEL

The two-center shell model was developed by the Frankfurt school for symmetric splitting [13] and for low asymmetry [14]. Here we present the main steps of the two-center shell model we developed for large asymmetry starting from another symmetrical two-center model [15].

The general Hamiltonian describing the evolution of the level scheme of the two-center shell model is based on two oscillators which split from an initial common oscillator. The usual spin-orbit interaction and the \mathbf{I}^2 term are constructed as depending on the mass asymmetry. Thus, the total Hamiltonian reads:

$$H = H_{osc} + V(\mathbf{1} \cdot \mathbf{s}) + V(\mathbf{I}^2) \quad (11)$$

where H_{osc} is the two-oscillator Hamiltonian, and $V(\mathbf{1} \cdot \mathbf{s})$ and $V(\mathbf{I}^2)$ are the spin-orbit and the \mathbf{I}^2 potentials.

A. The diagonalization basis

The oscillator part of the Hamiltonian, H_{osc} , is given in cylindrical coordinates by:

$$H_{osc} = -\frac{\hbar^2}{2m_0} \left[\frac{\partial^2}{\partial \rho^2} + \frac{1}{\rho} \frac{\partial}{\partial \rho} + \frac{1}{\rho^2} \frac{\partial^2}{\partial \phi^2} + \frac{\partial^2}{\partial z^2} \right] + V(\rho, z), \quad (12)$$

where the asymmetric two-center oscillator potential has the form:

$$V(\rho, z) = \frac{1}{2}m_0 \begin{cases} \omega_{\rho_1}^2 \rho^2 + \omega_{z_1}^2 (z + z_1)^2, & z < z_0 \\ \omega_{\rho_2}^2 \rho^2 + \omega_{z_2}^2 (z - z_2)^2, & z \geq z_0. \end{cases} \quad (13)$$

Here z_0 is the separation plane coordinate between the two asymmetric systems on the symmetry axis Oz. Since we consider the case of two asymmetric spheres, $\omega_{\rho_1} = \omega_{z_1} = \omega_1$ and $\omega_{\rho_2} = \omega_{z_2} = \omega_2$.

To obtain an appropriate basis for this system, we consider the intermediate case when $\omega_{\rho_1} = \omega_{\rho_2} = \omega_1$. Then the potential is:

$$V(\rho, z) = \frac{1}{2}m_0 \begin{cases} \omega_1^2 \rho^2 + \omega_1^2 (z + z_1)^2, & z < 0 \\ \omega_1^2 \rho^2 + \omega_2^2 (z - z_2)^2, & z \geq 0. \end{cases} \quad (14)$$

At this point the intermediate Hamiltonian is separable, and one gets the eigenfunctions [15]:

$$\Phi_m(\phi) = \frac{1}{\sqrt{2\pi}} \exp(im\phi) \quad (15)$$

for the axial degree of freedom and

$$R_{n_\rho|m|}(\rho) = \sqrt{\frac{2\Gamma(n_\rho + 1)\alpha_1^2}{\Gamma(n_\rho + |m| + 1)}} \exp\left(-\frac{\alpha_1^2 \rho^2}{2}\right) (\alpha_1^2 \rho^2)^{\frac{|m|}{2}} L_{n_\rho}^{|m|}(\alpha_1^2 \rho^2) \quad (16)$$

for describing radial motion where $\alpha_i = (m\omega_i/\hbar)$, $\Gamma(x)$ is the gamma function, and $L_{n_\rho}^{|m|}(x)$ is the Laguerre polynomial. As one knows, the oscillator energy for oscillations in the plane perpendicular on the symmetry axis is:

$$E_{\rho,\phi} = \hbar\omega_\rho(2n_\rho + |m| + 1) \quad (17)$$

where $\omega_\rho = \omega_1$.

Solving the third equation which accounts for oscillations along the symmetry axis, we have different solutions for the two regions of the nuclear shape. According to the z -dependent potential,

$$V(z) = \frac{1}{2}m_0 \begin{cases} \omega_1^2 (z + z_1)^2, & z < 0 \\ \omega_2^2 (z - z_2)^2, & z \geq 0 \end{cases} \quad (18)$$

where z_1 and z_2 are the centers of the heavy and light spherical fragments, respectively, one obtains the differential equations

$$\left[\frac{d^2}{dz^2} + \frac{2m_0 E_z}{\hbar^2} - \frac{m_0^2 \omega_1^2 (z + z_1)^2}{\hbar^2} \right] Z_{\nu_1}(z) = 0, z < 0 \quad (19)$$

$$\left[\frac{d^2}{dz^2} + \frac{2m_0 E_z}{\hbar^2} - \frac{m_0^2 \omega_2^2 (z - z_2)^2}{\hbar^2} \right] Z_{\nu_2}(z) = 0, z \geq 0. \quad (20)$$

At this point it is important to mention that the $z = 0$ plane is the intersection plane between the two systems with $\omega_{\rho_1} = \omega_{\rho_2}$, whereas the “real” intersection between the asymmetric spherical systems is at $z = z_0$. The solution for the z -dependent Hamilton equation will be:

$$Z_\nu(z) = \begin{cases} C_{\nu_1} \exp\left[-\frac{\alpha_1^2(z+z_1)^2}{2}\right] H_{\nu_1}[-\alpha_1(z+z_1)] & , z < 0 \\ C_{\nu_2} \exp\left[-\frac{\alpha_2^2(z-z_2)^2}{2}\right] H_{\nu_2}[\alpha_2(z-z_2)] & , z \geq 0 \end{cases} \quad (21)$$

where C_{ν_1} and C_{ν_2} are normalization constants, and $H_\nu(z)$ are the Hermite functions.

As can be seen from these results, four quantities need to be determined: the two quantum numbers ν_1 and ν_2 and the two normalization constants C_{ν_1} and C_{ν_2} . These quantities can be calculated from a system of four equations. From the normalization condition

$$\int_{-\infty}^{\infty} |Z_\nu(z)|^2 dz = 1, \quad (22)$$

from the continuity of the z -wave function and its derivative at $z=0$

$$Z_{\nu_1}(z=0) = Z_{\nu_2}(z=0), \quad (23)$$

$$Z'_{\nu_1}(z=0) = Z'_{\nu_2}(z=0), \quad (24)$$

and from the energy matching condition along the O_z axis

$$\hbar\omega_1(\nu_1 + 0.5) = \hbar\omega_2(\nu_2 + 0.5). \quad (25)$$

From these, a basis for diagonalization of the potential differences to obtain the real energy values can be calculated.

B. The asymmetric oscillator system

Once we have total wave functions, we have to determine differences between the diagonal Hamiltonian and the real one. First, the oscillator Hamiltonian has to provide the initial oscillator potential when there is only one heavy sphere (starting point). For this initial configuration the difference that needs to be diagonalized is

$$\Delta V^{sphere}(z) = \begin{cases} \frac{1}{2}m_0[\omega_1^2(z+z_1)^2 - \omega_2^2(z-z_2)^2] & , z \geq 0 \\ 0 & , z < 0. \end{cases} \quad (26)$$

For the next stages of deformation, the difference between the z -dependent oscillator potentials that needs to be diagonalized is:

$$\Delta V(z) = \begin{cases} 0 & , z < 0 \\ \frac{1}{2}m_0[\omega_1^2(z+z_1)^2 - \omega_2^2(z-z_2)^2] & , 0 \leq z \leq z_0 \\ 0 & , z > z_0. \end{cases} \quad (27)$$

As for the difference in the ρ -dependent oscillator potential, this only exists for intersecting spheres and is given by:

$$\Delta V(\rho) = \begin{cases} 0 & , z \leq z_0 \\ \frac{1}{2}m_0(\omega_1^2 - \omega_2^2)\rho^2 & , z > z_0 \end{cases} \quad (28)$$

or, if written as an operator, the quantity to be diagonalized is given by:

$$\Delta V(\rho) = \frac{1}{2}m_0(\omega_1^2 - \omega_2^2)\rho^2\Theta(z - z_0) \quad (29)$$

where $\Theta(z)$ is the Heaviside function. The difference $\Delta V(\rho)$ is zero for the initial spherical configuration.

Once $\Delta V(z)$ and $\Delta V(\rho)$ are diagonalized and added to the oscillator energy of the sphere + ellipsoid system, which is

$$E = \hbar\omega_1[2n_\rho + |m| + \nu_1 + 1.5], \quad (30)$$

the level schemes of the two intersecting asymmetric oscillators with frequencies ω_1 and ω_2 are obtained.

C. Spin-orbit and orbit-orbit interactions

The spin-orbit ($\mathbf{1} \cdot \mathbf{s}$) and orbit-orbit ($\mathbf{1}^2$) interaction terms generate the necessary single-particle level splitting to obtain the correct schemes of the individual fragments after separation.

The use of deformation dependent form of these operators has been introduced in [16] for the Nilsson model and in [14] for the two center shell model; instead of the \mathbf{l} operator one introduces:

$$\mathbf{l} = \frac{\nabla V \times \mathbf{p}}{m_0 \omega^2} \quad (31)$$

where V is the asymmetric two-center oscillator potential. The usual expression for the two operators are:

$$\begin{aligned} V(\mathbf{l} \cdot \mathbf{s}) &= -2\kappa \hbar \omega \mathbf{l} \cdot \mathbf{s} \\ V(\mathbf{l}^2) &= -\kappa \mu \hbar \omega \mathbf{l}^2. \end{aligned} \quad (32)$$

Since one obtains the level schemes of two nuclei which lie in different mass regions, the strength parameters of the interactions κ and μ will be different. The values we use for these parameters are:

$$\begin{aligned} \kappa_n &= 0.0588 & \kappa_p &= 0.0592 \\ \mu_n &= 0.328 & \mu_p &= 0.335 \end{aligned} \quad (33)$$

for actinide region, and for light nuclei region:

$$\begin{aligned} \kappa_n &= \kappa_p = 0.0601 \\ \mu_n &= \mu_p = 0.448. \end{aligned} \quad (34)$$

Since the strength parameters are different for the asymmetric regions of the nuclear shape, they become z -dependent operators as follows:

$$\begin{aligned} \kappa \cdot \hbar \omega(z) &= \kappa_1 \cdot \hbar \omega_1 + (\kappa_2 \cdot \hbar \omega_2 - \kappa_1 \cdot \hbar \omega_1) \Theta(z - z_0) \\ \kappa \mu \cdot \hbar \omega(z) &= \kappa_1 \mu_1 \cdot \hbar \omega_1 + (\kappa_2 \mu_2 \cdot \hbar \omega_2 - \kappa_1 \mu_1 \cdot \hbar \omega_1) \Theta(z - z_0). \end{aligned} \quad (35)$$

To obtain a Hermitian operator for $V(\mathbf{l} \cdot \mathbf{s})$ and $V(\mathbf{l}^2)$ one has to use the anticommutator [14]:

$$\begin{aligned} V(\mathbf{l} \cdot \mathbf{s}) &= - \left[\kappa \cdot \hbar \omega(z), \frac{\nabla V \times \mathbf{p}}{m_0 \omega^2} \mathbf{s} \right], \\ V(\mathbf{l}^2) &= -\frac{1}{2} \left[\kappa \mu \cdot \hbar \omega(z), \left(\frac{\nabla V \times \mathbf{p}}{m_0 \omega^2} \right)^2 \right]. \end{aligned} \quad (36)$$

For the dependence of κ and μ with respect to the elongation, we choose a linear dependence for the oscillator frequency along the z -axis:

$$\kappa_i = \kappa_0 + \frac{\omega_i - \omega_0}{\omega_{if} - \omega_0}(\kappa_{if} - \kappa_0) \quad (37)$$

and the same law of variation for μ . Here $i=1,2$, κ_0 is the value for the initial nucleus and κ_{if} for the final one.

Finally one has to diagonalize the potential:

$$\Delta V(\rho, z) = \Delta V(z) + \Delta V(\rho) + V(\mathbf{1} \cdot \mathbf{s}) + V(\mathbf{1}^2) \quad (38)$$

together with the diagonal term of the two-center oscillator potential. The model provides the evolution from an initial level scheme toward two asymptotically independent single-particle schemes. With the introduction of large asymmetry between fragments, the shapes can simulate the existence of a soliton on the nuclear surface and assign it a microscopic structure.

V. SHELL CORRECTIONS

The level scheme of a soliton shape is used to obtain the shell corrections of the system. As the soliton is assimilated with an emerging fragment, it will provide the shell correction value of the independent nucleus of similar shape. Shell corrections are obtained by means of the Strutinsky procedure [17]. One defines the shell correction energy as the difference between the total sum of the energy levels and a smoothed part of the spectrum:

$$\delta E = \sum_{\nu} 2E_{\nu} - \tilde{U}. \quad (39)$$

One calculates the smoothed part \tilde{U} with the help of a smoothed level density function $\tilde{g}(\epsilon)$, which is obtained by averaging the real distribution $g(\epsilon)$ over the whole energy spectrum:

$$\begin{aligned} \tilde{g}(\epsilon) &= \frac{1}{\gamma} \int_{-\infty}^{\infty} \zeta\left(\frac{\epsilon - \epsilon'}{\gamma}\right) g(\epsilon') d\epsilon' \\ &= \frac{1}{\gamma} \sum_{i=1}^{\infty} \zeta\left(\frac{\epsilon - \epsilon'}{\gamma}\right), \end{aligned} \quad (40)$$

where $\gamma = \Gamma/\hbar\omega$ and $\zeta(x)$ is the smoothing function. A common smoothing function is provided by

$$\zeta(x) = \frac{1}{\sqrt{\pi}} e^{-x^2} \sum_{k=0}^m a_{2k} H_{2k}(x), \quad (41)$$

where $H_n(x)$ are the Hermite polynomials. The coefficients a_{2k} are

$$a_{2k} = \frac{H_{2k}(0)}{2^{2k} \cdot (2k)!}. \quad (42)$$

The Fermi energy $\tilde{\lambda}$ of the smoothed level distribution is calculated as a solution of the particle number conservation:

$$N_p = 2 \int_{-\infty}^{\tilde{\lambda}} \tilde{g}(\epsilon) d\epsilon. \quad (43)$$

Then, the total energy of the uniform level distribution \tilde{U} , reproducing the microscopic part which is not subjected to local fluctuations of the spectrum, is obtained as:

$$\tilde{U} = 2\hbar\omega \int_{-\infty}^{\tilde{\lambda}} \tilde{g}(\epsilon) \epsilon d\epsilon. \quad (44)$$

After performing the calculations, one obtains the following formula, which can be used directly

$$\begin{aligned} \delta U = & \sum_{\nu} \{ \epsilon_{\nu} [1 - erf(x_{F_{\nu}})] \\ & + \frac{e^{-x_{F_{\nu}}^2}}{\sqrt{\pi}} \cdot [2\epsilon_{\nu} \sum_{k=1}^m a_{2k} H_{2k-1} + \tilde{\gamma} a_{2m} H_{2m}] \}, \end{aligned} \quad (45)$$

where $erf(x)$ is the error function. Usually one chooses the upper order of the Hermite polynomials to be $m=3$. The variable $x_{F_{\nu}}$ is given by

$$x_{F_{\nu}} = \frac{\epsilon_{\nu} - \epsilon_F}{\gamma}, \quad (46)$$

Shell corrections are calculated separately for protons and neutrons, and the results are added.

VI. RESULTS

A first look at the energetic behavior of an emerging soliton is given in Fig. 2 in terms of the macroscopic energy surfaces. The LHS macroscopic energy surface corresponds to the formation of ^{40}Ca on the surface of ^{248}No , whereas the RHS represents the ^{16}O -like soliton on the surface of ^{224}Th . Variation along the elongation R corresponds to the increment in the soliton amplitude along the symmetry axis. A larger neck radius R_3 corresponds to a larger half-width L . The rear plane at $R=0$ is the spherical state of the system. Then the energy increases monotonously with a higher slope for small values of the neck radius. As R_3 increases, the energy increase is smoothed by the necking. With the enhancement of the kinetic energy of the soliton the half-width becomes larger, except in the first stages of the process where the neck radius is very small. The ridge in energy has a maximum at the near touching spheres configuration for both reactions. The slope continues to increase for large R_3 , beyond the touching point value of the elongation R .

The addition of shell corrections yields the total deformation energy shown in Fig. 3. As a first observation note the pronounced deformed ground state of ^{248}No as the first minimum in energy moves to $R > 0$, and a much less but still deformed ground state for ^{224}Th . For both emerging solitons it is obvious that the energy path corresponds to large half-width values up to the top of the energy ridge; then they abruptly turn towards rupture point shapes ($R_3=0$). Hence, these potential energy surfaces suggest a three-dimensional curve as the path of minimum energy in the cluster emission. The potential barrier formed along the path of minimum energy values is obtained by minimization of the total energy in the multi-dimensional deformation space.

The static paths, which a soliton with the internal structure of an emitted cluster has to follow, have been plotted on the contour maps of the energy surface in (R, R_3) coordinate space in Fig. 4. Again the LHS plot is the ^{40}Ca emission, and the RHS one corresponds to ^{16}O . Apart from the first R values, where R_3 is small, the solitons bypass the first energy peak by taking large neck radius values, i.e. large half-widths. As the energy increases on

the large R_3 side, the static path for both cases changes direction reaching the scission point where the clusters are emitted.

The two barriers are plotted in Fig. 5 with a full line, together with the macroscopic energy (dotted line) and the shell corrections (dashed line). One can see how the deformed ground state of ^{248}No is formed (LHS plot): due to shell corrections, the first minimum is at about 6.8 MeV of the total energy. This point becomes the ground state and the whole barrier in front of the emerging soliton is shifted with respect to this value. A two-humped barrier no higher than about 1.2 MeV blocks the ^{40}Ca emission.

The situation is different for the emission of ^{16}O from ^{224}Th . The ground state is only slightly deformed. A rather high one-hump barrier of about 11 MeV extends along the whole range of elongation R up to the scission point. Shell corrections decrease slightly the macroscopic energy values. The decrease is mainly due to the double-magic character of ^{208}Pb which forms as the cluster emerges.

One can state that ^{40}Ca -like solitons are energetically favored to form on the nuclear surface of a very heavy nucleus as ^{248}No . The formation of ^{16}O -like soliton on ^{224}Th is not energetically favored due to the high and large potential barrier it has to penetrate.

The relative velocity distribution V of the two presumed solitons along the minimum energy path, together with the scaled values of the halfwidth L and the relative amplitude $a = A/R_1$, are plotted in Figs. 6. We investigated the evolution of these soliton parameters (as defined in section I), which are a function of the static energy evolution, parametrized by the distance between centers R .

In the first stages, the tendency is that the amplitude and half-width increase with the elongation parameter, when the emitted cluster is emerging out from the parent nucleus (since their non-overlapping sector is increasing). During the formation of the cluster the half-width remains practically constant, since the surface energy controls this stage. When the two nuclei are well separated, the soliton envelope hardly fits the two spheres, and in this limit, the half-width approaches zero value. This gives the limiting configuration for this soliton model. These values of the half-width L (solid line) are compared with

those obtained analytically in [3] directly from the soliton amplitude, within the frame of the nonlinear liquid drop model (L -dashed line). We notice a good agreement for the half-widths within the range $R \simeq 4.5 - 14$ Fm. The hydrodynamic soliton model is not valid anymore for separation parameter R smaller than 4-5 Fm, because of the dominating shell effects in this range. This can be noticed in a comparison between Fig. 2 and Fig. 3 for $R \leq 4 - 5$ Fm. For the first R values, the static paths follow the first energy peak, and jump from small toward large values for R_3 , Fig. 4, providing small half-widths (Figs. 6, L -solid line), while a pure hydrodynamic soliton would have larger half-widths for this range (L -dashed line). In the above range of validity of the soliton model, we calculate the relative velocity of the soliton (V -dashed line), [3]. The velocity is increasing with the amplitude of the soliton, hence with the elongation of the cluster-like emission shape. Fig. 6a displays the ^{40}Ca emission, and Fig. 6b represents the ^{16}O emission. Soliton shapes at the beginning and the end of the process are also shown. For lighter nuclei (like ^{16}O) the evolution of the parameters is smooth and monotonic. In the case of heavier nuclei (^{40}Ca) we obtained some oscillations in width and velocity, during the first half of the emission process, which can be related with the oscillations produced by the shell effects in the R_3 parameter.

This work was supported by the U.S. National Science Foundation through a regular grant, No. 9970769, and a Cooperative Agreement, No. EPS-9720652, that includes matching from the Louisiana Board of Regents Support Fund. RAG is grateful to Prof. J. P. Draayer for a postdoctoral appointment in the Department of Physics and Astronomy, Louisiana State University, Baton Rouge.

REFERENCES

- [1] C. Rebbi and G. Soliani, *Solitons and Particles* (Singapore, World Scientific, 1984); R. Rajaraman, *Solitons and Instantons* (North-Holland, Amsterdam, 1982).
- [2] G. N. Fowler, S. Raha and R. M. Weiner, *Phys. Rev.* **C31** (1985) 1515.
- [3] A. Ludu and J. P. Draayer, *Phys. Rev. Lett.* **80** (1998) 2125; A. Ludu, A. Sandulescu and W. Greiner, *J. Phys. G: Nucl. Part. Phys.* **23** (1997) 343.
- [4] A. Ludu *et al*, *J. Phys. G: Nucl. Part. Phys.*, **21** (1995) and L41.
- [5] V. G. Kartavenko, A. Ludu, A. Săndulescu and W. Greiner, *Int. J. Modern Phys.* **E 5** (1996) 329; A. Dhar and S. Das Gupta, *Phys. Rev.* **C30** (1984) 1545.
- [6] D. N. Poenaru and W. Greiner, in *Handbook of Nuclear Properties* (Oxford University Press, 1996) 375.
- [7] I. Bialynicki-Birula and J. Mycielski, *Ann. Phys.* **100** (1976) 62.
- [8] K. A. Gridnev and E. F. Hefter, *Phys. Lett.* **A77** (1980) 490.
- [9] R. Rajaraman, *Solitons and Instantons* (North-Holland, Amsterdam, 1987).
- [10] W. Scheid and W. Greiner, *Z. Phys.* **A226** (1979) 364.
- [11] H. J. Krappe, J. R. Nix and A. J. Sierk, *Phys. Rev.* **C20** (1979) 992.
- [12] D. N. Poenaru, M. Ivascu and D. Mazilu, *J. Phys.* **G5** (1979) 1093.
- [13] D. Scharnweber, U. Mosel and W. Greiner, *Phys. Lett.* **24B** (1970) 601.
- [14] J. Maruhn and W. Greiner, *Z. Phys.* **251** (1972) 431.
- [15] E. Badraxe, M. Rizea and A. Sandulescu, *Rev. Roum. Phys.* **19, 1** (1974) 63.
- [16] W. J. Rij and C. T. Hess, *Nucl. Phys.* **A142** (1970) 72.
- [17] V. M. Strutinsky, *Nucl. Phys.* **A95** (1967) 420.

Figure captions

Fig.1 Deformation space for two-center shell-model calculations. The neck radius R_3 can vary from zero (intersecting spheres) to infinity (compact shapes). R (the distance between the two centers) and R_2 (radius of the emitted fragment) are also independent coordinates.

Fig.2 Macroscopic potential energy surfaces for ^{40}Ca emission from ^{248}No (left-hand-side plot) and for ^{16}O emission from ^{224}Th (right-hand-side plot), as function of elongation R and neck radius R_3 . First maximum appears close to the touching point configuration in both cases ($R_3=0$).

Fig.3 Total potential energy surfaces (macroscopic plus shell corrections) for ^{40}Ca emission from ^{248}No (left-hand-side plot) and ^{16}O from ^{224}Th (right-hand-side plot). The deformed ground state of ^{248}No is revealed as a minimum along R_3 axis at its origin. For both surfaces the closest energy maximum occurs at the tangent sphere configuration. The maximum energy value for larger R_3 is not reached in the figure.

Fig. 4 Contour plot of Fig. 3 with static path (dashed line) for ^{40}Ca emission (left-hand-side plot) and ^{16}O emission (right-hand-side plot). As the elongation increases the amplitude of the soliton increases together with the half-width which is proportional to the neck radius R_3 . Once the touching point maximum is bypassed, both shapes decrease rather abruptly through necking towards scission.

Fig. 5 The barriers along the static path for ^{40}Ca emission (left-hand-side plot) and ^{16}O (right-hand-side plot), together with macroscopic energy (dotted lines) and shell corrections (dashed lines). Shell corrections increase the total energy of the first energy minimum for ^{248}No , thus the two-humped barrier is not higher than about 1.2 MeV. ^{16}O emission from ^{224}Th has a barrier of about 11 MeV.

Figs. 6 The evolution of $a = A/R_1$, L (with shell corrections solid line, and without shell corrections dashed line) and V parameters in relative units, versus the elongation R in fm. The corresponding nuclear configurations are plotted for two situations: for the initial stage

when the emitted cluster is only slightly displaced off the common center, and the final stage when the two nuclei are almost separated. Fig. 6a displays the ^{40}Ca emission and Fig. 6b the ^{16}O emission. In the later case, oscillations can be seen in the soliton parameters related to the shell corrections.

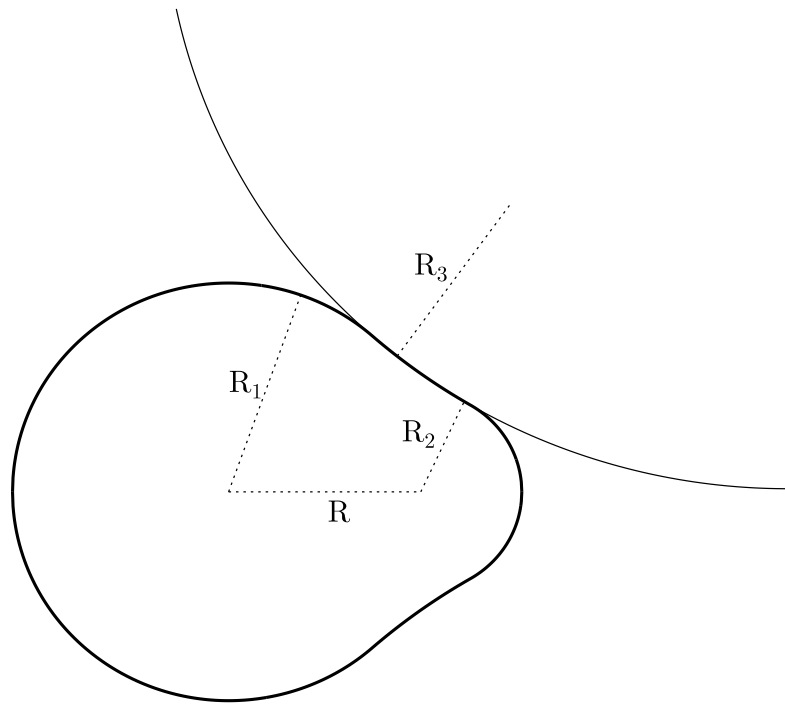


Fig. 1, Phys. Rev. C, Gherghescu *et al.*

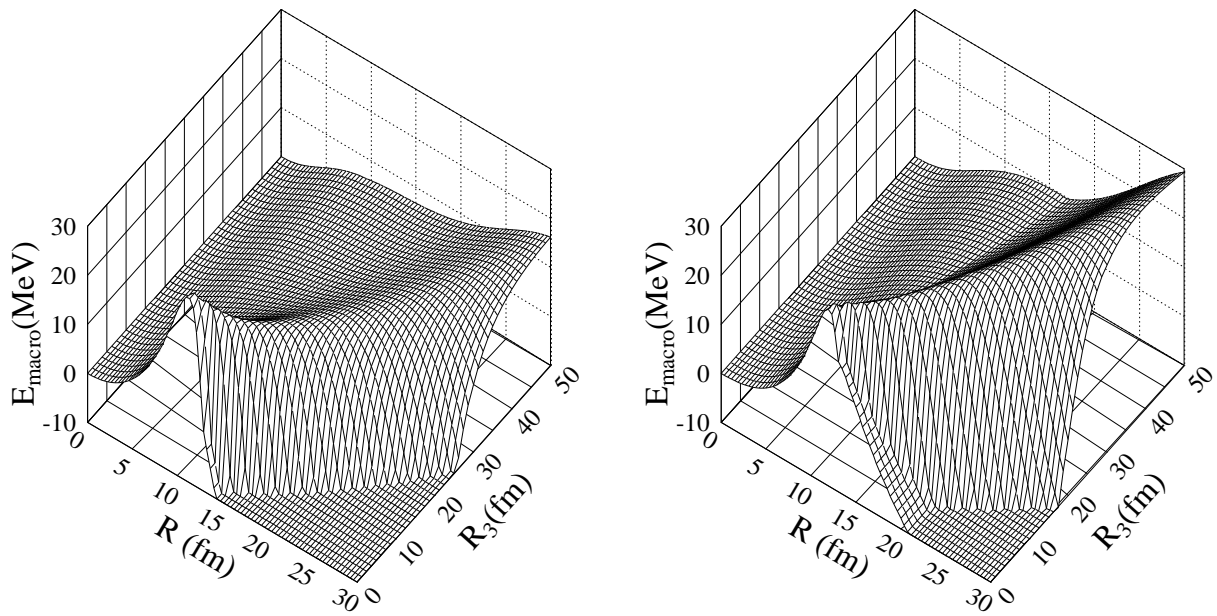


Fig. 2, Phys. Rev. C, Gherghescu *et al.*

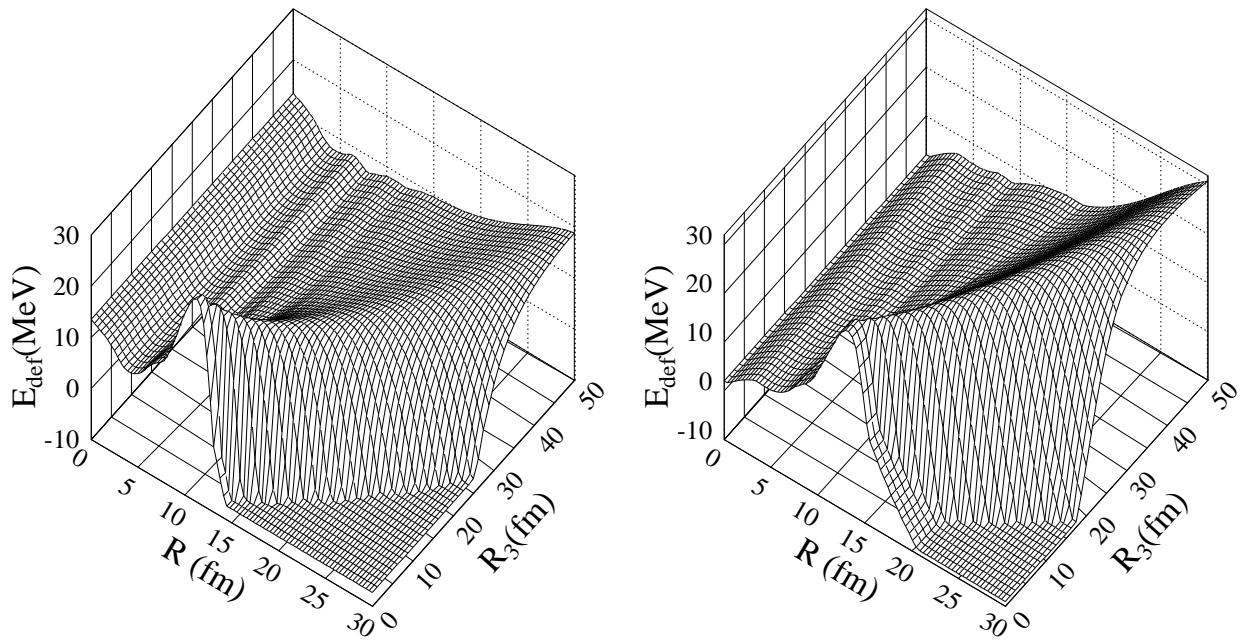


Fig. 3, Phys. Rev. C, Gherghescu *et al.*

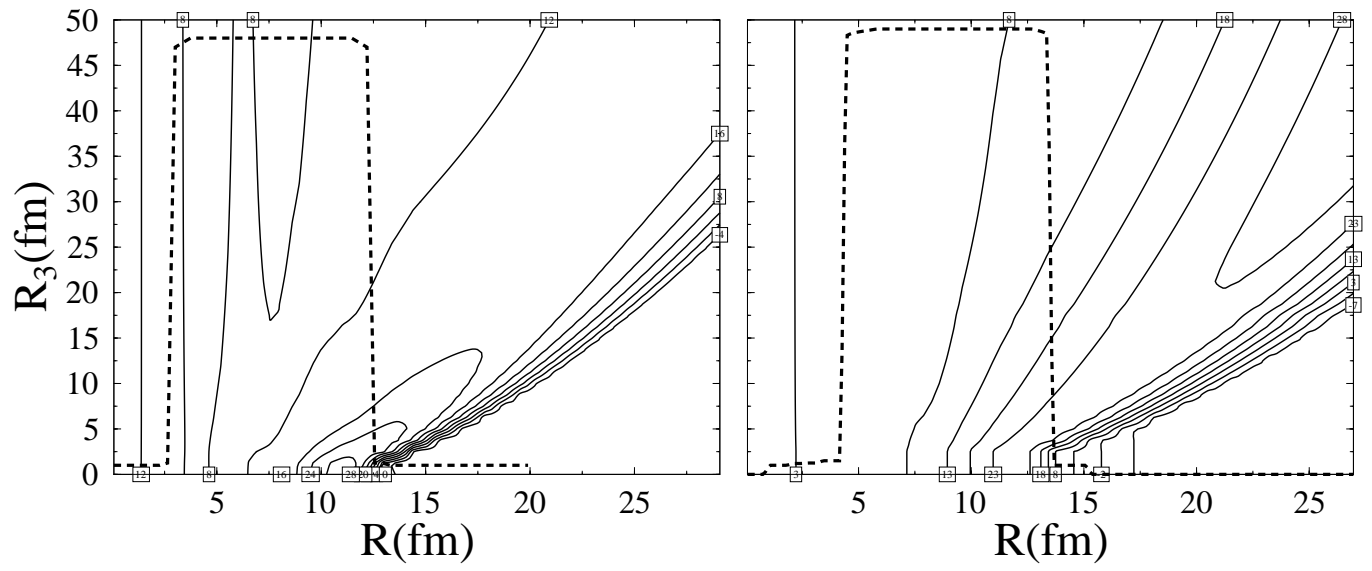


Fig. 4, Phys. Rev. C, Gherghescu *et al.*

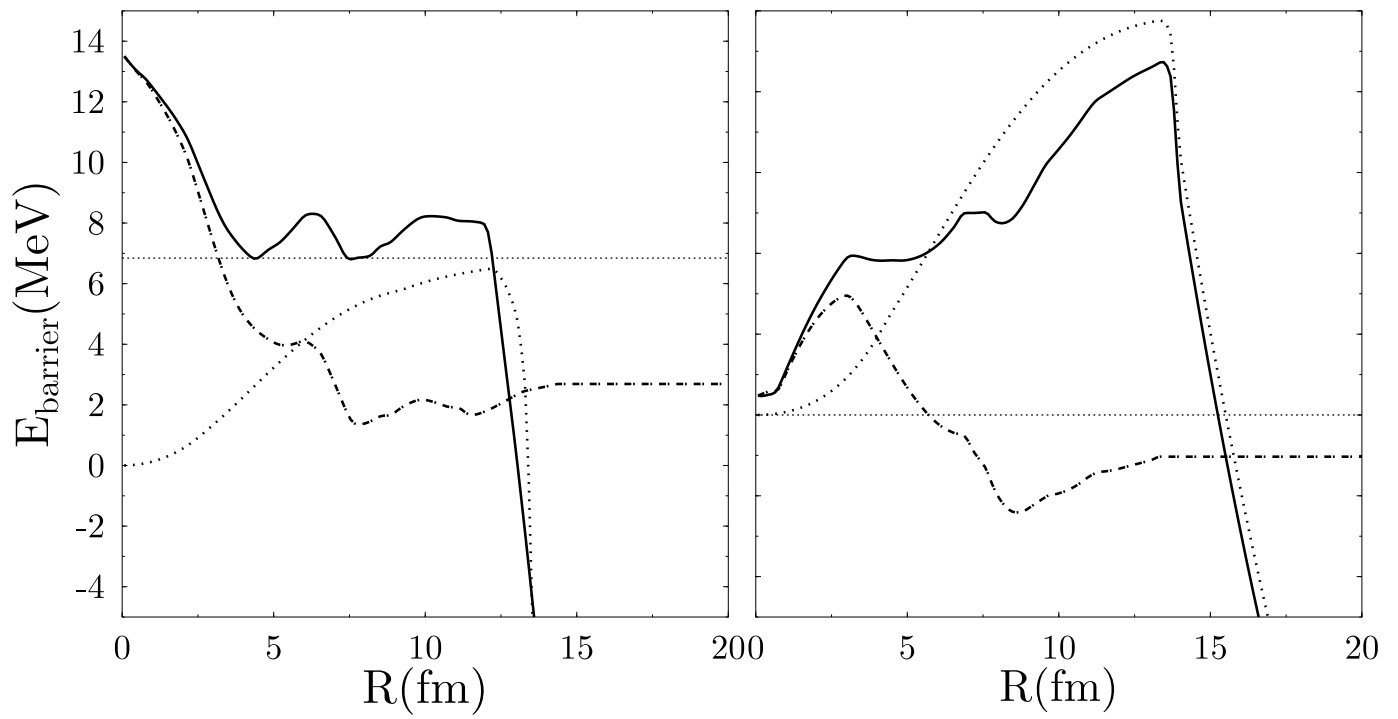


Fig. 5, Phys. Rev. C, Gherghescu *et al.*